Heliyon 10 (2024) e28544

Contents lists available at ScienceDirect

Heliyon

journal homepage: www.cell.com/heliyon

Research article

Using EEG total energy as a noninvasively tracking of intracranial (and cerebral perfussion) pressure in an animal model: A pilot study

Fernando Pose [a,1], Carlos Videla [b,1], Giovanni Campanini [a], Nicolas Ciarrocchi [b,2], Francisco O. Redelico [a,c,*,2]

[a] *Instituto de Medicina Translacional e Ingeniería Biomédica, CONICET-Hospital Italiano de Buenos Aires - Instituto Universitario del Hospital Italiano de Buenos Aires, Potosi 4265, Buenos Aires, C1199ACL, Argentina*

[b] *Servicio de Terapia Intensiva de Adultos, Hospital Italiano de Buenos Aires, Tte. Gral. Juan Domingo Perón 4190, Buenos Aires, C1199ACL, Argentina*

[c] *Departamento de Ciencia y Tecnologia, Universidad Nacional de Quilmes, Roque Sáenz Peña 352, Bernal, Pcia de Buenos Aires, B1876BXD, Argentina*

ARTICLE INFO

MSC:
46N30
62J99

Keywords:
EEG
Intracranial pressure monitoring
Intracranial hypertension
Additive generalized model

ABSTRACT

Purpose: This study aims to describe the total EEG energy during episodes of intracranial hypertension (IH) and evaluate its potential as a classification feature for IH. New methods: We computed the sample correlation coefficient between intracranial pressure (ICP) and the total EEG energy. Additionally, a generalized additive model was employed to assess the relationship between arterial blood pressure (ABP), total EEG energy, and the odds of IH. Results: The median sample cross-correlation between total EEG energy and ICP was 0.7, and for cerebral perfusion pressure (CPP) was 0.55. Moreover, the proposed model exhibited an accuracy of 0.70, sensitivity of 0.53, specificity of 0.79, precision of 0.54, F1-score of 0.54, and an AUC of 0.7. Comparison with existing methods: The only existing comparable methods, up to our knowledge, use 13 variables as predictor of IH, our model uses only 3, our model, as it is an extension of the generalized model is interpretable and it achieves the same performance. Conclusion: These findings hold promise for the advancement of multimodal monitoring systems in neurocritical care and the development of a non-invasive ICP monitoring tool, particularly in resource-constrained environments.

1. Introduction

Intracranial hypertension (IH) is a frequently encountered clinical condition in neurocritical care patients, which often requires urgent medical intervention and, in certain cases, surgical treatment [1]. This condition can have devastating consequences because

* Corresponding author at: Instituto de Medicina Translacional e Ingeniería Biomédica, CONICET-Hospital Italiano de Buenos Aires - Instituto Universitario del Hospital Italiano de Buenos Aires, Potosi 4265, Buenos Aires, C1199ACL, Argentina.
E-mail address: francisco.redelico@hospitalitaliano.org.ar (F.O. Redelico).

[1] Both author share the first autorship.

[2] Both author share the last autorship.

https://doi.org/10.1016/j.heliyon.2024.e28544
Received 29 July 2023; Received in revised form 18 March 2024; Accepted 20 March 2024

Available online 26 March 2024

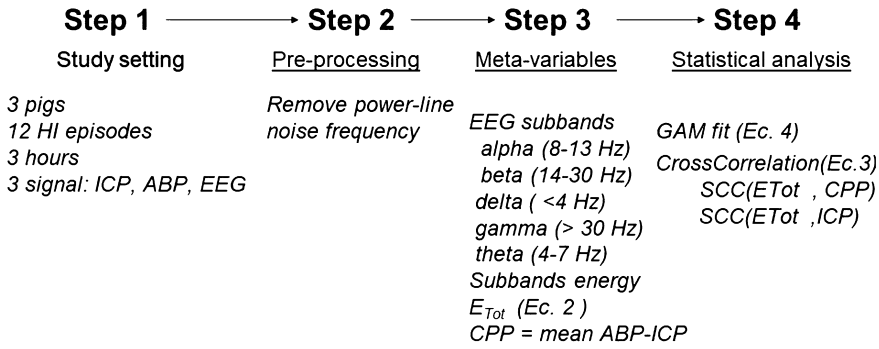

Fig. 1. Schematic representation of the presented analysis.

it leads to secondary brain damage due to a drop in cerebral perfusion pressure (CPP) and subsequent decrease in cerebral blood flow (CBF), particularly in patients with compromised cerebral autoregulation [2].

ICP management must be personalized for each patient and at each moment in a holistic view, including structural and temporal variability, as well as host-specific responses to treatments [1].

To accomplish this, the utilization of multimodal monitoring (MM) that incorporates information regarding the patient's neurological state is fundamental. MM allows us to determine alterations in cerebral oxygenation or metabolism, facilitating personalized treatment and reducing the risk of secondary brain injury [3].

The electroencephalogram (EEG) is a relatively inexpensive, noninvasive, portable method that provides real-time monitoring of electric brain activity [4]. Several studies have investigated the relationship between ICP and EEG experimentally, sometimes reaching with contradictory results. Stein [5] observed a decrease in EEG frequencies in unanesthetized cats with an increase in intracranial pressure. However, in [6] found no apparent correlation between intracranial pressure measured in the intraventricular space and EEG in twenty-six adult cats. Forster [7] observed a decrease in amplitude in the intermediate range of EEG frequencies and the loss of higher frequencies. Langfitt and collaborators [8] presented an experimental model of IH in monkeys using a balloon insufflation in the extradural space, and they observed immediate changes in the EEG, primarily localized in the region surrounding the balloon when a rapid insufflation was generated. These experimental studies employed methods not recommended for intracerebral pressure measurement, did not have statistical analysis and employed different experimental models that do not allow comparison with each other. Additionally, a significant limitation is the difficulty in quantifying and interpreting the results in real time. Therefore, the use of quantitative EEG (qEEG) can be useful to observe real-time changes in neurological activity in real time and facilitate its interpretation. qEEG is a time-compressed simplified display derived from mathematical and analytical techniques applied to the raw EEG signal [9].

The main objectives of this article, presented as a proof of concept, are twofold. Firstly, it seeks to evaluate the changes in total energy and the evolution of different EEG sub-bands in relation to variations in intracranial pressure (ICP) and cerebral perfusion pressure (CPP), based on a previous porcine experiment conducted by the research group. Secondly, it aims to assess the feasibility of incorporating the total energy of the EEG into a machine learning tool, specifically a generalized additive model, and explore its potential utilization as an alarm in a multimodal monitoring system for neurocritical patients.

2. Materials and methods

In Fig. 1, we present a schematic representation of the analysis conducted in this article.

- Step 1: Data is obtained from a previously published animal experiment [10], consisting of 60,000 samples of ICP, ABP, and EEG obtained during 12 HI episodes in 3 pigs, as described in [10] and summarized in *subsection 2.1* and *Appendix A*.
- Step 2: The data has been filtered and pre-processed as explained in *subsection 2.2.1* and *Appendix A.3*.
- Step 3: Meta-signals, i.e., signals derived from the originally observed ones, such as CPP, EEG sub-bands, and their respective energies, are calculated as described in *subsection 2.2*.
- Step 4 is explained in *subsection 2.2.3 Cross-Correlation Coefficient* and in *2.3 Generalized additive model and classification performance*.

In the Appendix D, Table D.4, we present a checklist based on the *ARRIVE guidelines 2.0* to allow the reader to assess the reliability of the findings [11].

2.1. Intracranial pressure experiment

The data analyzed in this article come from an animal experiment carried out at the *Hospital Italiano de Buenos Aires*, in compliance with all Argentinean laws. The experimental protocol was approved by the Institutional Committee for the Care and Use of Laboratory Animals of the *Instituto de Medicina Translacional e Ingeniería Biomédica* under protocol number 0007/19. Although a comprehensive

explanation of the experiment was provided in [10], in Appendix B, we present the key aspects related to the rationale behind the experimental design, animal preparation, induction of intracranial hypertension, and data acquisition. This approach ensures the self-contained nature of the present paper.

The sample frequency was 200 Hz for EEG and 120 Hz for ICP and femoral arterial blood pressure, which were subsequently resampled at 200 Hz.

2.2. EEG features calculation

2.2.1. EEG preprocessing

The EEG signals were initially filtered using a band-stop Butterworth filter to remove the power-line noise frequency at 50 Hz, specific to Argentina. Subsequently, each EEG was decomposed into 5 sub-bands using a band-pass Butterworth filter based on their frequency ranges: alpha (8-13 Hz), beta (14-30 Hz), delta (<4 Hz), gamma (>30 Hz) and theta (4-7 Hz). The filter order was 4 for all filters used. Finally, the statistics, i.e. the EEG total energy and the Energy corresponding each sub-band, were estimated over each filtered sub-band using a sliding rectangular window of 3 seconds (600 samples) and a shift of 1 second (200 samples) between each pair of windows. As shown in Appendix B, a strong correlation was observed among all EEG electrodes, possibly attributed to the small brain size of the pig. Therefore, all correlation calculations were performed between ICP (CPP) and the total energy (E_{Tot}) calculated from the C3 electrode, which is closest to the lesion caused by the Foley catheter. In any case, to estimate the GAM we have used all the electrodes, because although the trends are similar, their absolute values are not.

2.2.2. EEG energy

We defined EEG_{α}, EEG_{β}, EEG_{δ}, EEG_{γ} and EEG_{θ} as the energy contribution, measured in μV^2, of each EEG sub-band and E_{Tot} as the total EEG Energy, measured also in μV^2.

The E_{Tot} is calculated as,

$$E_{Tot}(w) = EEG_{\alpha}(w) + EEG_{\beta}(w) + EEG_{\delta}(w) + EEG_{\gamma}(w) + EEG_{\theta}(w) \tag{1}$$

Where w represents the EEG sliding windows and the energy in each band for each sliding windows is calculated as

$$E_r(w) = \sum_{n=1}^{N} EEG^2_{(w,r)} \tag{2}$$

Where r represents one of the EEG sub-bands and n refers to the n-th sample within the w-slicing window and N stands for the length of the respective window.

2.2.3. Cross-correlation coefficient

In order to evaluate the correlation between two different signals, the Sample Cross-Correlation coefficient (SCC) (9) is often computed. The SCC measures the similarity between a time series (X) of length T and lagged versions of another time series (Y) as a function of the lag ($k = 0, \pm1, \pm2, \pm T-1$) and it is calculated as

$$SCC(k)_{(X,Y)} = \frac{C(k)_{XY}}{s_X s_Y}, \tag{3}$$

Where C_{XY} represents the cross-covariance between X,Y with lag k, and s_X and s_Y are the sampled standard deviations of variable X and Y defined as $s_X = \sqrt{((C_(X,X)(k=0)))}$ and $s_Y = \sqrt{((C_(Y,Y)(k=0)))}$, respectively. In our case we will evaluate the CSS between the Total Energy (X in equation (3)) and the ICP or (CPP) (Y in equation (3)).

2.3. Generalized additive model and classification performance

Unlike the previously explained tools, with the GAM, our interest is not focused on the trends of Energy in relation to the trends of PIC. Instead, we aim to study whether the absolute values of the former can be used to predict whether the PIC is above 20 mmHg (which we will refer to as positive instances) or below 20 mmHg (which we will refer to as negative instances), so we can use a regression approach.

Since each electrode measures local cortical electrical activity while ICP is a global variable, we can consider the information from the 8 electrodes in each pig as representing compatible electrocortical activity associated with a specific combination of ICP and ABP. Although Appendix B demonstrates a high correlation among most of the electrodes, the instantaneous values provided by E_{Tot} differ across electrodes. Therefore, we have a total of 24 distinct electrodes (8 electrodes × 3 pigs), resulting in 60,800 samples.

Unlike the previously presented methods, our current focus is not on studying the trends of E_{Tot} in relation to ICP. Instead, our objective is to determine whether the instantaneous value of E_{Tot} can predict if the instantaneous ICP value is greater (positive instance) or lower (negative instance) than 20 mmHg. Since each electrode measures local cortical electrical activity while ICP is a global variable, we can consider the information from the 8 electrodes in each pig as representing compatible electrocortical activity associated with a specific combination of ICP and ABP. Although Appendix B demonstrates a high correlation among most of the electrodes, the instantaneous values provided by E_{Tot} differ across electrodes. Therefore, we have a total of 24 distinct electrodes (8 electrodes × 3 pigs), resulting in 60800 samples.

These samples were randomly divided into two sets: 42560 samples (70% of the total) for the training set and 18240 samples (30% of the total) for the test set. A generalized additive model (GAM) [12] was fitted in the training set and used to predict the corresponding test set. Various metrics were calculated, including accuracy, balanced accuracy, recall, F1-score, sensitivity, specificity, area under the ROC curve (AUC), and precision of the test set, all of them are explained in Appendix C. The accuracy and balanced accuracy were also calculated using a 5-fold cross-validation scheme. This procedure was repeated ten thousand times, resulting in ten thousand possible models. Only the models for which the null hypothesis of non-significance was rejected at a significance level of 0.05 were analyzed.

A GAM is a statistical approach that is used to model nonlinear relationships between a response variable and multiple predictor variables. GAMs extends the capabilities of Generalized Linear Models (GLMs) by allowing for capturing more flexible and complex relationships between the response variable and the predictors. The extension of the usual linear model is possible using smoothing functions, such as splines [13], to model the relationship between the predictor variables and the response variable instead of a linear relationship as in traditional GLMs. Our proposed model is

$$log(p/(1-p)) = \mu + \beta_{ABP} \times ABP(w) + \beta_{E_{Tot}} \times E_{Tot}(w) + s(ABP(w)) + s(E_{tot}(w)) + \epsilon_i \quad (4)$$

In the equation, p represents the probability of the response variable being equal to 1, indicating the likelihood of the event (ICP > 20 mmHg) occurring. The term $log(p/(1-p))$ corresponds to the logarithm of the odds ratio, which is the ratio of the probability of success (ICP > 20 mmHg) to the probability of failure (ICP < 20 mmHg), ranging from 0 to infinity. The rectangular windows w refer to the segments or intervals over the ABP, E_{tot} are calculated. The right part of the equation is divided into two components: the parametric component and the nonparametric component. In the parametric part, β_0 represents the general mean, while β_{ABP} and $\beta_{E_{Tot}}$ represent the parameters associated with ABP and E_{Tot}, respectively. These parameters capture the linear relationship between the predictor variables and the response variable.

In the nonparametric part, $s(ABP)$ and $s(E_{Tot})$ represent the additive contributions of ABP and E_{Tot} to the response, respectively. The function $s(\cdot)$ represents a smooth function that characterizes the relationship between the independent variables and the response. In this case, a thin plate spline function with a maximum of 3 degrees of freedom was used to model the nonparametric components. The GAM model (4) was implemented using the 'gam' package [14] in R software [15].

3. Results

In accordance with the materials and methods outlined above, we conducted a comprehensive analysis of EEG characteristics during a total of 12 intracranial hypertension events observed in three pigs experiments. Our analysis encompassed the temporal evolution of the EEG, the correlation between the EEG energies and ICP (or CPP) and the power of E_{tot} as an ICP states classificator.

3.1. Temporal evolution of EEG and ICP (CPP)

Fig. 2 shows the temporal evolution of ICP (represented by solid blue line), CPP (represented by a dashed blue line) and the total energy of the EEG (E_{tot}, Eq. (1)) (represented by a solid red line). The EEG signals were recorded using the C3 electrode for three different pigs: pig 1, pig 2 and pig 3, as shown in Fig. 2.a, Fig. 2.b and Fig. 2.c, respectively. Based on visual examination of the figure, it is evident that when ICP increases during each episode, E_{tot} decreases. A contrasting behavior is observed in relation to CPP. Specifically, the energy of the EEG exhibits improvement when ICP decreases and CPP increases, as expected. The contribution (in absolute values) of each EEG rhythm is depicted in Fig. 3(I-III) for pig 1,2 and 3 respectively and presented numerically in Table 1. It is shown that E_{Tot} (light blue dashed line) is primarily influenced by the energy of the Delta and Theta rhythms (computed according to Eq. (2)). The contributions of the Alpha, Beta, and Gamma rhythms seem to have only a minor impact on E_{Tot}. This observation is further supported by the data presented in Table 1. The table presents the contribution of each rhythm (expressed as a percentage of E_{Tot}) during both the baseline and hypertension plateau periods within each generated episode. To evaluate the statistical significance of the differences between the energy levels of the two states for each rhythm and episode, we used the Wilcoxon signed-rank test. Most of the differences were found to be statistically significant at a 5% significance level, except for the cases marked with (*) in Table 2.

The median contributions during the baseline periods were 8% for alpha, 2% for beta, 69% for delta, 0.14% for gamma and 20% for theta rhythms, respectively. Similarly, during the intracranial hypertension plateau, the median contributions were 7% for alpha, 2% for beta, 73% for delta, 0.15% for gamma and 18% for theta rhythm, respectively.

3.2. CrossCorrelation between EEG and ICP (CPP)

In Table 2, we present the maximum SCC between E_{Tot} (Eq. (1)) and ICP as well as CPP. The correlations between ICP and E_{Tot} at lag 0 are all negative, indicating an inverse relationship between ICP and E_{Tot}, as observed in Fig. 2. The maximum correlation coefficient is -0.8 (episode J), while the minimum is -0.33 (episode B). Only one episode (episode E) does not exhibit a statistically significant correlation. Only two episodes (episodes A, I) show the maximum correlation at lag 0. In five episodes (episodes B, C, D, E, F), the maximum correlation occurs at negative lags, indicating that changes in ICP precede changes in E_{Tot}. In other five episodes (episodes G, H, J, K, L), the lag is positive, suggesting that changes in E_{Tot} precede changes in ICP. The median value of the coefficients with negative lag is -0.66, while for positive lag, it is -0.75. Considering the maximum lag instead of the correlation

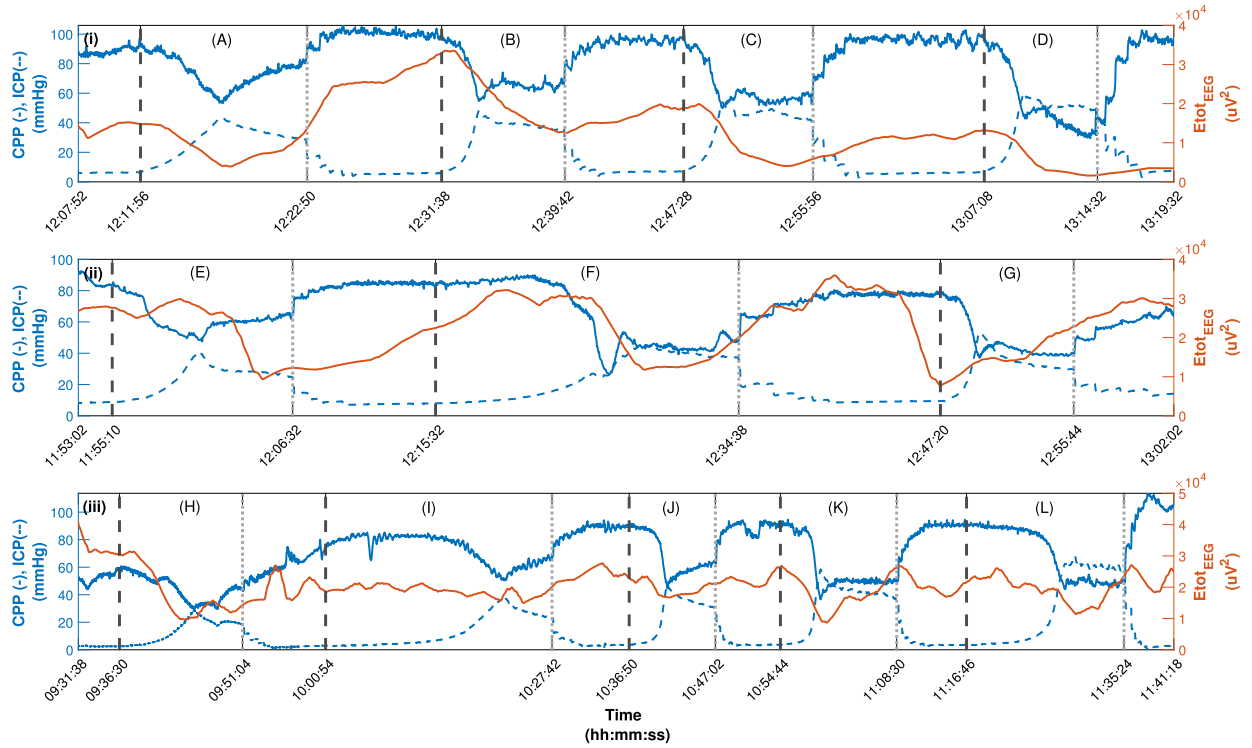

Fig. 2. Intracranial pressure (ICP, blue solid line), cerebral perfusion pressure (CPP, blue dashed line), and total EEG energy (E_{Tot}, Eq. (1)) (red solid line) for pigs 1, 2 and 3 in a top, middle and bottom subplots, respectively. The y-axis on the left side represents the values for ICP and CPP, while the y-axis on the right side represents the values for E_{Tot} Energy. Each episode between each pig is named with latin capital letters. There is a recovery time between two successive episodes marked by solid black vertical lines. Each episode is generated by the inflation and deflation of a balloon in the brain parenchyma. The indicated hours correspond to the actual hours at the time of the experiment.

Table 1
Contribution (in percentage) of each EEG subband energy (Eq. (2)) for the baseline and hypertension plateau periods in each episode for the experimental pigs.

Episode	Periods									
	Baseline					Plateau				
	alpha	beta	delta	gamma	theta	alpha	beta	delta	gamma	Theta
A	4	1	79	0.35	15	4	2	80	0.7	13
B	4	1	82	0.18	14	2	1	90	0.2	7
C	3	1	82	0.26	13	3	2	88	0.6	7
D	3	2	80	0.35	14	5	4	77	1.3	13
E	19	3	53	0.16	25	18	3	55	0.2	23
F	18	2	52	0.20	26	17	3	56	0.3	24
G	12	2	66	0.12	20	12	2	65	0.1	21
H	9	1	63	0.04	27	7	2	68	0.1	23
I	11	2	61	0.07	26	13	2	60	0.1	24
J	8	1	67	0.06	24	5	1	77	0.1	17
K	7	2	70	0.08	20	9	2	72	0.1	19
L	6	1	75	0.08	17	7	1	74	0.1	18

at lag 0 results in an 11% increase in correlation. Regarding the correlations between CPP and E_{Tot} given in lag 0, all coefficients are positive indicating a direct relationship between CPP and E_{Tot}. The maximum correlation coefficient is 0.92 (episode A), while the minimum is 0.4 (episode B). However, two episodes (episodes E, G) do not exhibit a statistically significant correlation. Only two episodes (episodes a, i) show the maximum correlation at lag 0. There are six episodes (episodes B, C, D, E, F, H) where the maximum correlation occurs at negative lags indicating that changes in CPP precede changes in E_{Tot}. Four episodes (episodes G, J, K, L) have a positive lag, suggesting that changes in E_{Tot} precede changes in CPP. The median value of the coefficients with negative lag is 0.54, while for positive lag, it is 0.56. However, when comparing the maximum coefficient with the one at lag 0, there is a 20% improvement in using the maximum coefficient.

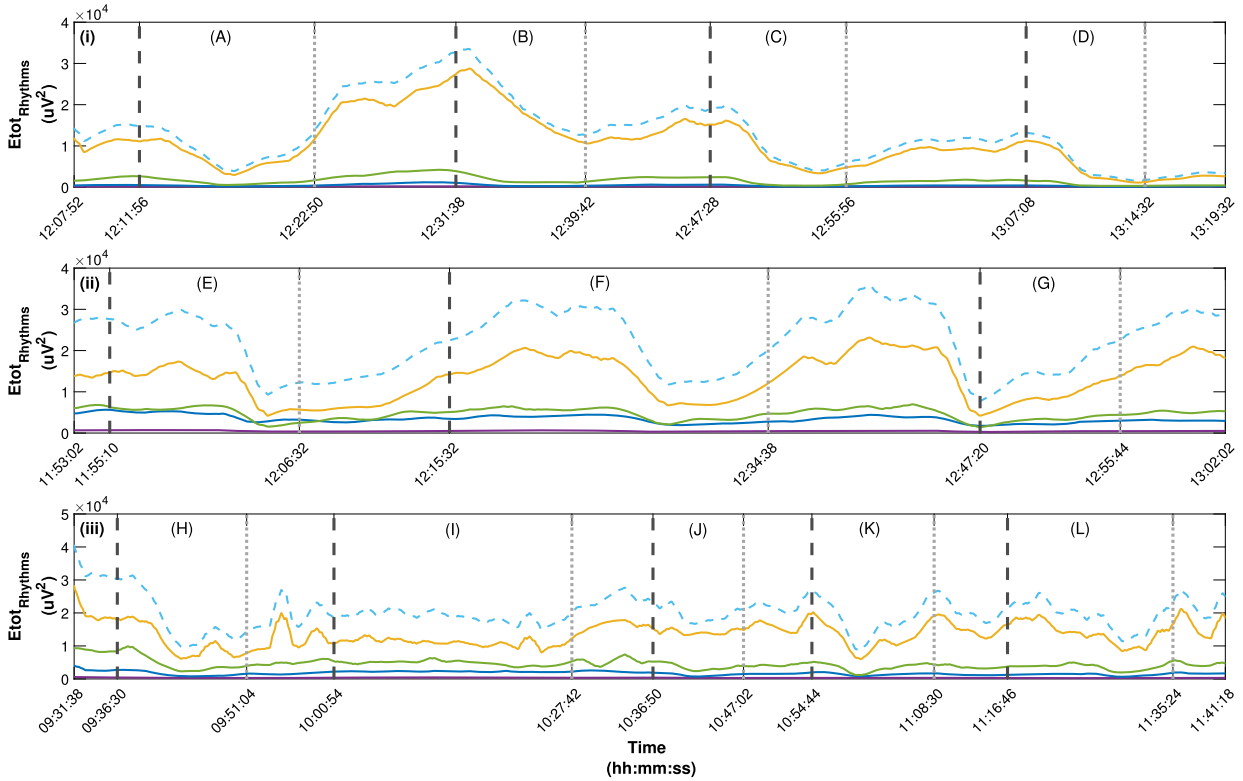

Fig. 3. Energy for each EEG subbands (Eq. (2)). Delta (yellow), Theta (green), Alpha (blue), Beta (purple) and the Total Energy (E_{Tot}, dashed light blue line). The subplots (a), (b) and (c) correspond to pigs 1, 2, 3, respectively. As in Fig. 2, each episode between each pig is named with latin capital letters and there is a recovery time between two successive episodes marked by solid black vertical lines. The indicated hours correspond to the actual hours at the time of the experiment.

Table 2
Maximum Sample Cross-Correlation Coefficient (SCC) between Total Energy E_{tot} (Eq. (1)) and ICP (column 2), Lag at maximum SCC (eq. (3)) (column 3), SCC at Lag 0 (column 4) and for CPP (column 5), Lag at maximum SCC (column 6), SCC at Lag 0 (column 7) for each episode (column 1) as marked in Fig. 2. All SCC values are statistically significant at 0.05, except for those marked with (*).

Episode	ICP			CPP		
	Max SCC	Lag	SCC at 0 lag	Max SCC	Lag	SCC at 0 lag
A	-0.77	0	-0.77	0.92	0	0.92
B	-0.62	-73	-0.33	0.69	-66	0.40
C	-0.71	-41	-0.57	0.71	-40	0.58
D	-0.66	-44	-0.49	0.65	-37	0.54
E	0.77	-173	-0.16(*)	0.77	-173	-0.16(*)
F	-0.76	-25	-0.74	0.73	-46	0.65
G	-0.76	81	-0.38	0.69	93	0.15(*)
H	-0.75	10	-0.74	0.45	-11	0.45
I	-0.39	0	-0.39	0.52	0	0.52
J	-0.90	31	-0.80	0.89	24	0.81
K	-0.74	30	-0.65	0.67	32	0.57
L	-0.70	62	-0.59	0.73	71	0.55

3.3. Predictive power of E_{Tot} for identifying ICP states

We followed the procedure outlined in section 2.3 and selected only the models for which we rejected the null hypothesis of the McNemar's Test on the confusion matrix, i.e., ACC > NIR. Out of the ten thousand models evaluated, only three thousand seven hundred and fifty-eight models met this condition.

A necessary step is to evaluate whether these models exhibit overfitting, which refers to fitting the noise in the data rather than the true underlying data, thus limiting their ability to generalize results to new data. To assess this, we calculated the accuracy and balanced accuracy, accounting for any class imbalance, for both the train and test sets, and subtracted them in each iteration. Fig. 5 illustrates the differences between these two measures. When subtracting the accuracy values (Fig. 5, left), we obtained an empirical

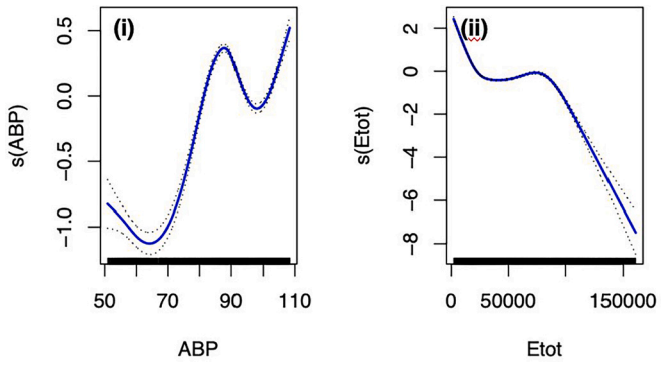

Fig. 4. The nonparametric main effect analysis of two factors: E_{Tot} (i) and arterial blood pressure (ABP) (i) including their respective credible intervals. The units on the x-axis correspond to the physical quantities represented, while the y-axis is dimensionless.

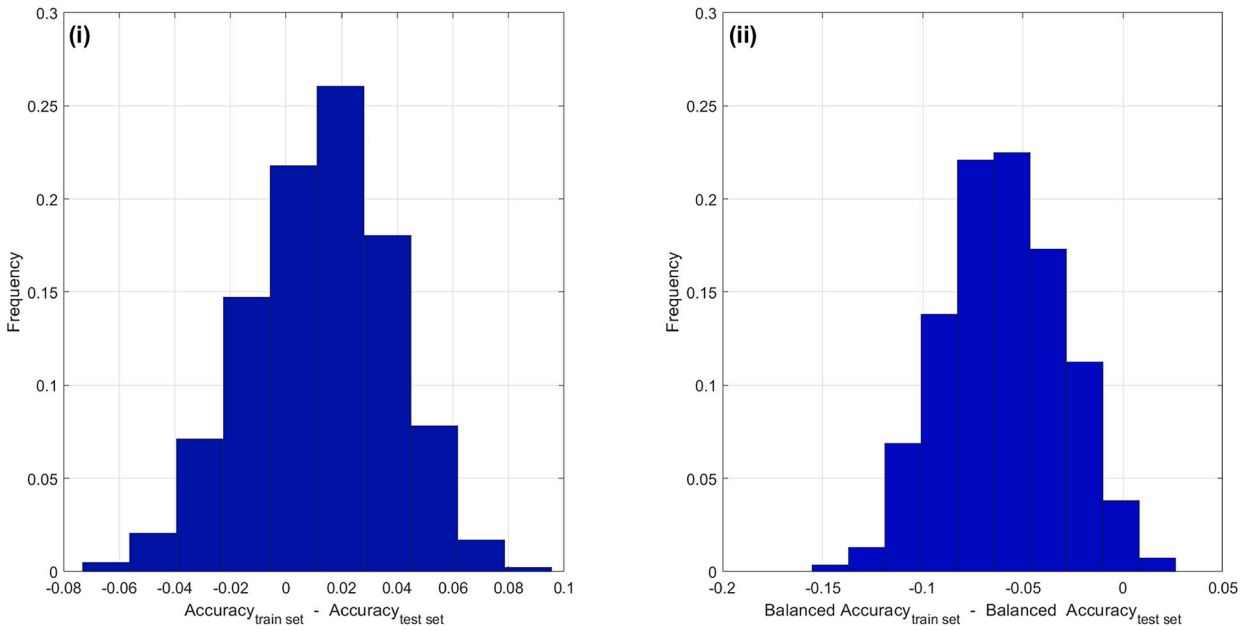

Fig. 5. Histograms illustrating the difference in (i) accuracy and (ii) balanced accuracy, calculated between the train and test sets for each iteration.

distribution with a mean of 0.01, a standard deviation of 0.02, a median of 0.01, a first quartile of -0.0051, a third quartile of 0.03 and a skewness of -0.17. In contrast, when subtracting the balanced accuracy (Fig. 5, right), the empirical distribution exhibited the following statistics: a mean of -0.05, a standard deviation of 0.03, a median of -0.06, a first quartile of -0.08, a third quartile of -0.03, and a skewness of 0.004.

Fig. 6 illustrates the performance measures of the classification for all interactions in the test set. The following metrics are presented: accuracy (median: 0.70, IQR: 0.02), precision (median: 0.55, IQR: 0.07), recall (median: 0.53, IQR: 0.15), F1 score (median: 0.54, IQR: 0.06), and AUC (median: 0.71, IQR: 0.03).

Fig. 7 shows a heatmap of the pairs (sensitivity, specificity) (x-axis, y-axis) for each interaction. The color scale varies from dark blue, indicating 0 occurrences of that combination to light yellow representing 231 occurrences. Sensitivity ranges from 0.27 to 0.80, with a median (IQR) of 0.53 (0.15), while specificity ranges from 0.60 to 0.96, with a median (IQR) of 0.79 (0.10).

Finally, Fig. 4, shows the plot for the nonparametric effect in a fitted GAM model with the following performance metrics: accuracy = 0.6388, sensitivity = 0.71, specificity = 0.60 and AUC = 0.70. In Fig. 4(left), the effect of the ABP variable on the odds of ICP exceeding 20 mmHg is shown. The odds range from -1.5 to 0.5. Between the ranges of 50-80 and 85-105, ABP appears to have a protective effect against hypertension. Between 80 and 85, the odds of observing ICP > 20 mmHg are positive. However, it is worth noting that the effect of ABP on the odds is considerably smaller compared to that of E_{Tot}, as illustrated in Fig. 4(right). The odds range varies from -8 to 2, and for values beyond 30000, the odds of ICP > 20 mmHg become negative.

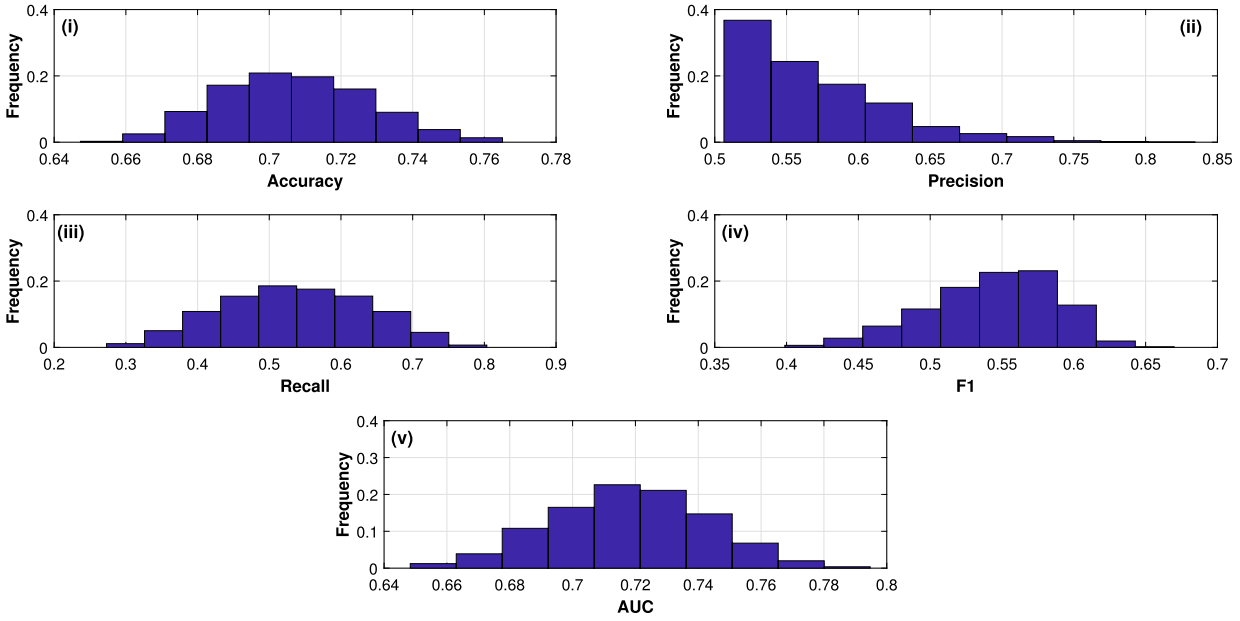

Fig. 6. Histograms illustrate the distribution of accuracy (i), precision (ii), recall (iii), F1 score (iV), and AUC (v) calculated for each iteration on the test set.

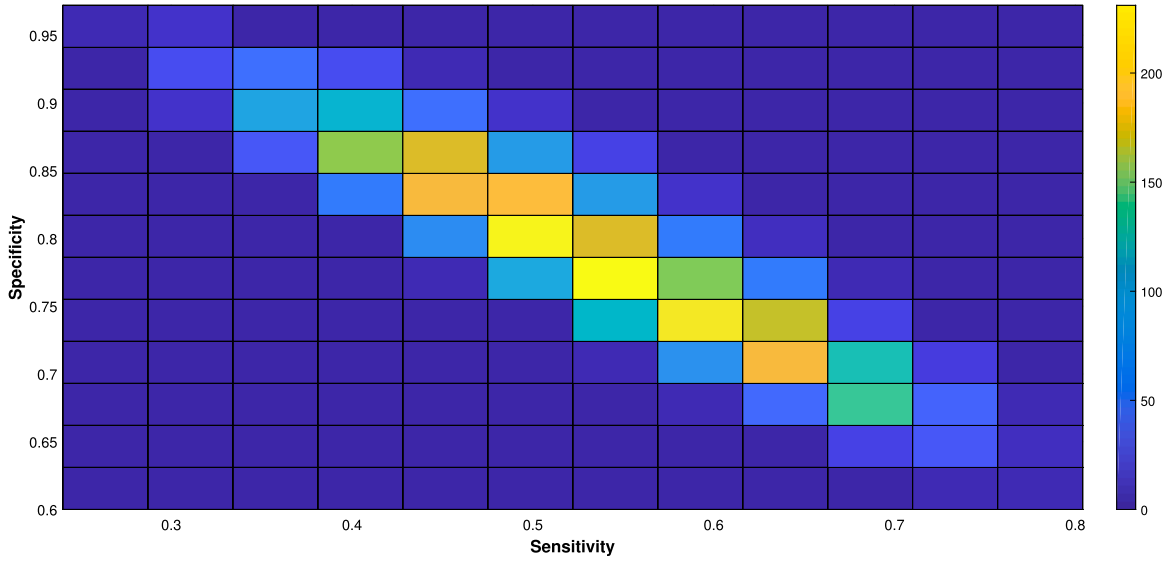

Fig. 7. Heatmap illustrates the sensitivity (x-axis) and specificity (y-axis) values calculated for each iteration on the test set.

4. Discussions

This contribution introduces a model that serves as an initial exploration into the use of EEG as a non-invasive method for estimating intracranial pressure, emphasizing its role as a proof of concept. The practical application of this model in clinical settings is not yet within immediate reach. While invasive measurement of intracranial pressure is recommended, it comes with potential complications, such as infections and hematomas, and is not universally accessible. A recent Synapse study [16] highlighted that nearly 50% of patients with acute brain injuries are not subject to invasive monitoring, with the lack of availability being a significant contributing factor. In a recent survey conducted in Latin America [17], it was observed that 53% of respondents opt for invasive monitoring, with only 7% applying it universally to patients with severe traumatic brain injuries. This underscores the urgency of developing non-invasive, complication-free, and cost-effective methods for intracranial pressure estimation, especially considering the limited cases undergoing invasive monitoring in clinical practice.

To the best of our knowledge, there is currently no established standard animal model for investigating intracranial hypertension and its correlation with EEG. The preceding studies present variations that may initially seem contradictory, as discussed in the intro-

duction. However, it's important to note that these experiments are outdated and do not adhere to recommended methodologies for measuring intracranial pressure, lacking sophisticated statistical analyses, as proposed in this study. Undoubtedly, the methodology employed in generating intracranial hypertension and measuring intracranial pressure plays a pivotal role. In this investigation, we utilized an intraparenchymal measurement catheter, a currently recommended approach for invasive measurement of intracranial pressure, and the elevation method has been substantiated through various publications [10,18–20].

The time evolution of ICP (CPP) and the E_{Tot} is shown in Fig. 2. In Fig. 2.a (first pig), a progressive decline E_{Tot} over time and an interesting phenomenon of hysteresis as the decrement of E_{Tot} matches closely with ICP elevation (CPP decrement), but the recovery of E_{Tot} is delayed and incomplete following the restoration of baseline ICP (and CPP). This observation may indicate brain damage. In contrast, Fig. 2.b shows the second pig, which exhibits a lag with E_{Tot} decrement occurring much later than CPP and ICP changes during the first and second ICH episodes. However, during the last episode in the same pig, it seems that the E_{Tot} falls before the ICP elevation even begins. This discrepancy could be due to the accumulated brain damage from previous episodes. This accumulated damage at the beginning of each episode could be analogue to the heterogeneity of brain damage seen in patients admitted to a neurocritical care unit.

One could argue that electroencephalographic modifications may result from the inflation and deflation of the balloon, either directly through some mechanical effect or indirectly due to the necrosis produced. However, while there is a possibility that the inflation of the balloon alters the results of the electrodes closest to it due to the necrosis of the tissue, the same changes, in the variation in E_{Tot}, were observed in all electrodes, even those furthest from the balloon (see Fig. 2). Thus, if there were an alteration attributable to the balloon, it is local, minor, and unlikely to have modified the overall results. We can conclude that the EEG alteration was more likely due to intracranial hypertension or reduced cerebral perfusion pressure.

The sample Cross-Correlation Coefficient between E_{Tot} and ICP (and CPP) suggests that E_{Tot} is inversely correlated with ICP and directly correlated with CPP. In particular, the correlation with CPP is stronger, with a coefficient of 0.92, compared to the coefficient of -0.8 with ICP. This stronger correlation with CPP could be attributed to the ischemic process that occurs as a secondary response to the elevation of intracranial pressure, influencing E_{Tot}. In some episodes, the absence of a significant correlation at lag 0 may be due to the presence of noise in the EEG data or the existence of a delayed ischemic process from previous episodes.

The observation that EEG changes precede ICP changes in 41% of episodes and CPP changes in 50% of episodes suggests the potential influence of factors not accounted for in our analysis. This pattern aligns with findings in [21,22], where paroxysms preceded an increase in ICP due to vascular coupling. According to their explanation, the heightened demand for oxygen during paroxysms leads to vasodilatation and subsequent ICP elevation. However, in our study, we did not identify paroxysms preceding the rise in ICP induced by balloon inflation. Consequently, the observed effects may not be directly attributed to the neurovascular coupling described in [23]. While paroxysms were not found before ICP elevation, we did observe instances where ICP elevation sometimes preceded electroencephalographic modifications, and at other times, occurred in the reverse order. This divergence could stem from an unknown or minimally studied compensation and coupling mechanism. Alternatively, it might be attributed to the temporal averaging employed in both our article and [21,22]. These averages may obscure the true onset of the impact on the two signals, causing ICP to seemingly precede or lag behind EEG intermittently, suggesting a potential mathematical artifact. It's crucial to emphasize that these findings do not undermine the robustness of the results obtained with the GAM or the validity of the cross-correlations, including those reported in [21,22]. Nevertheless, the observed divergence may be noteworthy, as it may reveal unexplored neurovascular coupling mechanisms that, to our knowledge, may not have been investigated to date.

Although there are episodes where the maximum correlation is not reached at lag 0, the improvement in correlation by considering the highest coefficient is relatively small, with an improvement of 11% for the correlation with ICP and 20% for the correlation with CPP. For these, E_{Tot} could be considered a suitable biomarker for incorporation into a Multimodal monitoring system. This would allow for the monitoring of different physiological variables in order to personalize treatment in neurocritical patients [1] as reflects the neural damage from the ICP raises (or CPP deterioration).

The EEG Energy (dashed light blue line in Fig. 3) is primarily influenced by the Delta Rhythm (yellow line in Fig. 3), followed by the Theta Rhythm (green line in Fig. 3) across all pigs. This observation further supports the idea presented in [24] that the changes in EEG activity during hypertension predominantly occur at medium frequencies. Additionally, in our case, it is possible that higher-frequency rhythms are decreased due to the sedation administered during the experiment, which is a commonly observed phenomenon in routine clinical practice. Nevertheless, given the small difference in the powers of the alpha, beta, and gamma bands between the baseline and hypertension periods, we believe that while statistical significance is present, this difference lacks clinical significance.

A prospective study involving 21 neurocritical patients with head trauma and subarachnoid hemorrhage further supports the aforementioned relationship [21]. In their analysis, they used the relative spectral power for each frequency band (Delta, Theta and Alpha), and also employed spectral entropy. Through the application of the Granger test to evaluate causality, they found that in most cases there is a strong causal influence between both variables. This study is significant as it is one of the initial investigations to demonstrate this relationship in humans. However, the authors acknowledge certain limitations, particularly regarding the potential influence of sedative drugs, antiepileptic drugs, and medications used for IH treatment on the EEG recordings may therefore have influence on this relationship. To mitigate these biases, we developed an experimental study that involved generating IH events without the administration of treatment drugs and maintaining stable anesthetic drug doses. Similar to the aforementioned study, we have also observed a strong relationship between ICP and EEG in our experimental setting. Recently, there has been a recognized need to incorporate additional variables in ICP monitoring [1]. As illustrated in Fig. 1, not all episodes of intracranial hypertension exhibit the same energy. Consequently, E_{tot} decreases during each hypertensive period. As a result, baseline periods with normal

Table 3
Point-wise (and confidence interval) for maximum and minimum Accuracy, Sensitivity, Specificity, Precision, F1-score, and AUC obtained in the models presented in [27] along with the obtained with the proposed GAM.

Feature	Min	Max	GAM
Accuracy	0.70 (0.62,0.78)	0.77 (0.69,0.85)	0.70 (0.68,0.72)
Sensitivity	0.49 (0.31,0.67)	0.65 (0.49,0.81)	0.53 (0.51,0.55)
Specificity	0.79 (0.67,0.91)	0.92 (0.85,0.98)	0.79 (0.76,0.81)
Precision	0.64 (0.46,0.83)	0.87 (0.75,0.98)	0.56 (0.55,0.58)
F1-score	0.50 (0.35,0.65)	0.58 (0.42,0.74)	0.54 (0.52,0.56)
AUC	0.74 (0.64,0.85)	0.86 (0.78,0.93)	0.71 (0.69,0.74)

ICP, at the end of the experiment, have E_{Tot} values lower than those at the beginning of the experiment. Therefore, E_{Tot} could be a candidate for summarizing the cerebral damage caused by the elevation of ICP or the reduction of CPP.

An important aspect of neuromonitoring has received limited attention is the potential utilization of EEG as a non-invasive measure for monitoring ICP. This is particularly significant in resource-limited regions or situations where traditional non-invasive monitoring methods, such as transcranial Doppler [25] or optic nerve sheath measurements [26], can not be employed due to cost constraints, lack of trained personnel, or other limitations. In this context, we are exploring the possibility of employing the E_{Tot} derived from EEG signals not as a direct surrogate for ICP, but rather as a tool for classifying ICP levels above or below a specific threshold, such as 20 mmHg. Although E_{Tot} may not serve as the definitive variable for ICP assessment, its potential for classification makes it a promising candidate for inclusion into machine learning algorithms or as an alert system for identifying episodes of elevated intracranial pressure.

To our knowledge, the only published study on using EEG as a classifier for ICP is [27]. In this study, various machine learning techniques, including Logistic Regression (LR), Naive Bayes (NB), Random Forest (RF), and Support Vector Machine (SVM), were employed to evaluate different variables as classifiers of ICP below or above the threshold of 25 mmHg. In our study, we utilized a modeling approach known as the Generalized Additive Model (GAM). Unlike more data-dependent and generalization-focused methods commonly associated with machine learning, GAM is closely aligned with the classical linear regression model—a fundamental pillar of traditional statistics. The distinctive strength of GAM over linear regression lies in its ability to ease the assumption of linearity, opting instead for a non-parametric fit. In our specific application, we implemented a spline basis within the GAM framework.

As a general guideline, [28] recommend a minimum sample size of at least 10 observations per parameter included in a linear model. In our model, which comprises the intercept, the parameter for ABP, and corresponding parameters for E_{tot}, we possess a dataset consisting of more than 42,560 observations. This ample dataset ensures that we have a sufficiently robust foundation for estimating the involved parameters.

In Table 3, we present the maximum and minimum values (along with their 95% confidence intervals) of selected classification performance measures as reported in [27], as well as the results obtained with the GAM model. We observe that the precision, sensitivity, and F1-score of the GAM model are not statistically different from those achieved by the best model in [27]. However, in the remaining performance indicators, our results fall between the highest and lowest performances, indicating that our approach does not surpass the highest performance but also does not perform worse than the lowest performance. It is worth noting that, except for LR (Logistic Regression), the models presented in [27] lack interpretability. One notable advantage of GAMs is their ability to maintain interpretability through the non-parametric component of the model and its relationship with the odds of the independent variables. In our model (see Fig. 4), we observe the protective effect of E_{Tot} when its value exceeds 35000, as well as the influence of ABP within the ranges of 50 mmHg to 80 mmHg and 85 mmHg to 105 mmHg. Therefore, an alarm could be generated whenever these parameters deviate from these values.

In [29], a retrospective analysis was conducted on the records of 100 patients with various pathologies, including traumatic brain injury, subarachnoid hemorrhage, or intracerebral hemorrhage conditions to compare the ability of several methods, namely nerve sheath diameter, pulsatility index, estimated ICP using transcranial Doppler, and neurological pupil index measured using automated pupillometry, as classifiers for intracranial hypertension, the reported area under the curve (AUC) values for each of these methods are presented, they are 0.78 (95% CIs 0.68-0.88) for ONSD, 0.85 (95% CIs 0.77-0.93) for PI, 0.86 (95% CIs 0.77-0.93) for eICP, and 0.71 (95% CIs 0.60-0.82) for NPI. It can be observed that the AUC of our GAM model is 0.71 (95% CIs 0.69,0.74), indicating no statistically significant difference with respect to these methods.

5. Limitations

One limitation of our study is that it was conducted using an animal model rather than human subjects. Although pigs were selected due to their anatomical similarities to humans, it is crucial to acknowledge that there may still be inherent differences between species. However, previous studies have suggested that pigs can provide valuable insights into human physiology and allow for translation of data and conclusions to humans [30,31].

The cyclic nature of the experiment could be a confounding factor that affects the results, as the electrical activity does not fully recover during the periods between two hypertensive events. The purpose of the experiment was not to simulate any pathophysiological process but to induce controlled intracranial hypertension and observe its potential impact on the electroencephalogram.

Although it is known that intracranial hypertension episodes in humans do not exhibit this cyclic nature and resolve within short time periods, we have developed this cyclic model to minimize the use of animals in accordance with the principles of animal research, namely Replacement, Reduction, and Refinement [32–34]. Additionally, each episode of intracranial hypertension has its own steady-state period. Another limitation is the number of cases analyzed; nevertheless, we believe that identifying patterns in 12 episodes provides a valid proof of concept. Regarding the data acquisition technique, the EEG is highly susceptible to ambient noise, and its energy depends on the depth at which the electrodes are placed. Therefore, it is crucial to develop a fixation method, such as a headband, as an integral part of the monitoring system. All experiments were carried out in a laboratory, where noise sources such as artificial respirators, monitors, and anesthetic machines were present; however, the noise levels were lower compared to those in the intensive care unit.

6. Conclusions

While the mechanisms underlying the relationship between intracranial pressure and cortical electrical activity, as measured by surface electroencephalogram, are not fully elucidated, our study has demonstrated the feasibility of real-time assessment of neuronal activity changes associated with variations in ICP or CPP using quantitative electroencephalography. This discovery underscores the potential incorporation of EEG as part of a multimodal monitoring system for neurocritical patients. E_{tot}, being capable of quantitatively reflecting electroencephalographic modifications induced by elevated ICP or decreased CPP, provides valuable information for monitoring potential brain damage in neurocritical patients. Nevertheless, further research is warranted to investigate the impact of sedative drugs, potential spatial effects in humans, and the underlying genesis of this relationship.

CRediT authorship contribution statement

Fernando Pose: Investigation. **Carlos Videla:** Investigation. **Giovanni Campanini:** Investigation. **Nicolas Ciarrocchi:** Supervision, Investigation. **Francisco O. Redelico:** Supervision.

Declaration of competing interest

The authors declare that they have no known competing financial interests or personal relationships that could have appeared to influence the work reported in this paper.

Data availability

Data will be made available on request.

Appendix A. Description of the experiment

A.1. Animal preparation

The experimental model was developed in three previously healthy 6-month-old Landrace pigs, each weighing an average of 25-30 kg. The animals were premedicated with ketamine at a dose of 15 mg/kg and xylazine via intramuscular injection administered by the veterinarian. General anesthesia was induced through an atrial vein using 6 mg/kg fentanyl, 4 mg/k propofol, and 1.2-1.5 mg/kg rocuronium. Intubation was performed using a 7.0 mm cuffed tube. Anesthesia was maintained throughout the experiment with a continuous intravenous infusion of propofol at a rate of 0.25-0.30 mcg/kg/min, remifentanil at a rate of 0.5 mcg/kg/min, and pancuronium at a rate of 0.04 mg/kg/h. Mechanical ventilation was performed in a pressure-controlled mode with a positive pressure at the end of the expiration of 5 cmH2O and a FiO2 of 0.40. The respiratory rate and tidal volume were adjusted to maintain normocarbia, which was monitored using a spirometer. Normovolemia was maintained by infusing a complete electrolyte solution at a rate of 10-15 ml/kg/h. All anesthesia procedures were performed by contracted veterinarian anesthesiologists.

A.2. Intracranial hypertension induction

IH was induced by inserting 8 French 2-Way Pediatric Foley Catheter (Well Lead Medical®, China) into the brain parenchyma, through a burr hole located 20 mm anterior to the coronal suture and 15 mm lateral to the sagittal suture, on the side opposite to the placement of an ICP catheter (Codman® Intracranial Pressure Monitor). In a subsequent necropsy studies, the intraparenchymal lesion produced by the inflation of the balloon was observed. [10] The IH events were carried out as follows:

- Induction of IH: A 0.9% saline solution was infused using a continuous infusion pump into a balloon to achieve different slopes of ICP rise until the desired ICP value was reached.
- Maintenance: Once the target value was reached, it was maintained stable for 5 minutes, if the clinical conditions allowed.
- Pressure drop: The balloon was deflated at a rate of 1 ml per minute until it was completely empty.
- Rest: After the balloon was emptied, it remained deflated for 10 minutes.

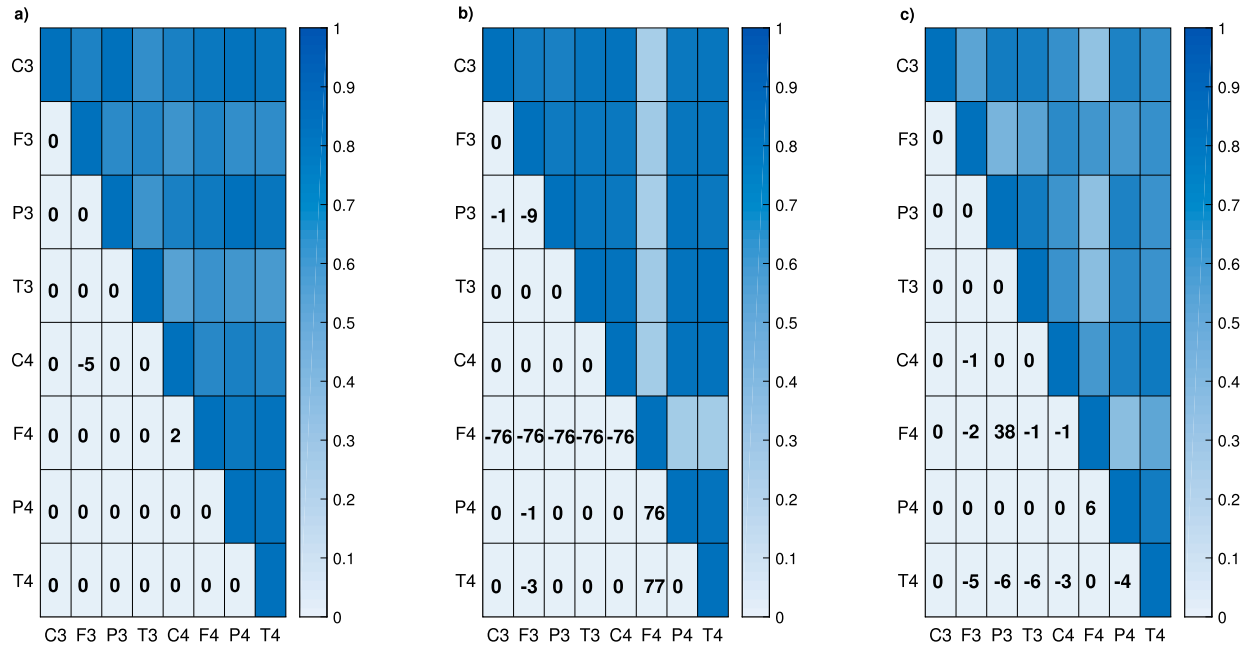

Fig. B.8. Upper triangular matrix presents the maximum sample cross-correlation coefficient (Eq. (3)) between E_{Tot} (Eq. (1)) of the EEG electrodes in the i-th column and j-th row. The corresponding color code indicates the strength of the correlation. Lower triangular matrix shows the lag (highlighted in bold) associated with the cross-correlation.

This protocol was repeated until the desired number of IH events was obtained. After all the events were completed, an IH event was induced with the objective of reaching cerebral circulatory arrest (CPP less than 5 mmHg), which was maintained for 1 hour. Subsequently, the animals were sacrificed by administering an intravenous overdose of propofol (20 mg/kg) and fentanyl (10 mg/kg), followed by the administration of 40 ml of a 19.1% potassium chloride solution. Before the first balloon insufflation and between any two episodes, the balloon remained deflated, resulting in normal ICP. These periods were referred to as steady-state episodes.

A.3. Data acquisition

During the experiment, data from ICP, femoral blood arterial pressure (ABP) and 8-channel EEG were recorded. EEG signals were recorded using a Neurovirtual PSG/EEG equipment model BWII (Fort Lauderdale, FL), and the signal processing was conducted using BMWAnalysis software. The EEG was continuously recorded using 8 electrodes placed at F3, F4, C3, C4, P3, P4, T3, and T4 with reference to the arithmetic average of electrodes A1 and A2, following the 10–20 system nomenclature. ICP was recorded using Codman Express Intracranial pressure (ICP-Codman-Raynham-MA, USA). Numeric and waveform data, including ICP and ABP, from the Philips Intellivue monitor MP70 (Philips Healthcare Inc., Andover, MA) were downloaded using custom-made software based on the open-source application VSCaptureMP, which is part of the VSCapture software suite [35]. All recorded biosignals and data were synchronized with the local area network clock of the hospital. CPP was calculated by subtracting the mean ABP (mABP) and the mean ICP (mICP), i.e., $CPP = mABP - mICP$. The sample frequency was 200 Hz for EEG and 120 Hz for other signals, which were subsequently resampled at 200 Hz.

Appendix B. E_{Tot} spatial configuration

The maximum cross-correlation of E_{Tot} between each pair of electrodes within the same pig is presented in the upper triangular matrices shown in Fig. B.8. The high correlation observed may be attributed to the small size of the pig's brain, indicating that it is possible to analyze the EEG data recorded solely at the C3 electrode, as we have done in this paper. Additionally, it is shown that electrodes F4 and P4 exhibit considerable noise in pig 2 (Fig. B.8.b) and to a lesser extent in pig 3 (Fig. B.8.c). The lag at which the cross-correlation is observed is presented in the lower matrices in Fig. B.8.

Appendix C. Statistical analysis metrics for the prediction model

To evaluate the performance of our classification model, we comparing our results with the results presented in [27] employing the following metrics:

- Accuracy is a widely used performance metric in classification models. It quantifies the proportion of correct predictions, both positive and negative, out of the total number of predictions made by the model. A high accuracy value indicates that the model has a good overall performance and is capable of making correct predictions for both the positive and negative classes.

$$Accuracy = \frac{TP + TN}{TP + TN + FP + FN} * 100 \tag{C.1}$$

- Sensitivity, also referred to as recall or true positive rate, is a metric used to evaluate a classification model's ability to correctly identify positive instances of a specific class. In our study, the positive instances correspond to the presence of intracranial hypertension. A high sensitivity value indicates that the model effectively detects positive cases.

$$Sensitivity = \frac{TP}{TP + FN} * 100 \tag{C.2}$$

- Specificity is a metric that assesses the performance of a classification model in correctly identifying negative instances of a specific class, such as the absence of intracranial hypertension in our study. A high specificity indicates that the model is effective at detecting negative instances.

$$Specificity = \frac{TN}{TN + FP} * 100 \tag{C.3}$$

- Precision is a metric that assesses the performance of a classification model in correctly identifying positive instances of a specific class. In our study, precision measures the model's ability to accurately detect cases of intracranial hypertension. A high precision value indicates that the model is effective in precisely identifying positive cases.

$$Precision = \frac{TP}{TP + FP} * 100 \tag{C.4}$$

- F1-Score is a measure that combines precision and sensitivity of the model into a single performance metric. In our study, It provides a balanced evaluation of the model's ability to correctly identify positive cases of intracranial hypertension, taking into account both false positives and false negatives. A high F1-Score value indicates that the model is effective in accurately identifying positive cases of intracranial hypertension.

$$F1 = 2 * \frac{Precision * Sensitivity}{Precision + Sensitivity} * 100 \tag{C.5}$$

- Receiver Operating Characteristic (ROC) curve is a graphical representation of the performance of a binary classification model. It is created by plotting the True Positive Rate (TPR) against the False Positive Rate (FPR) at various threshold settings. The area under the ROC curve (AUC) is a commonly used metric to quantify the overall performance of a classification model where a higher AUC indicates better overall performance of the model across different threshold settings.

Appendix D. Summary of the experimental procedure

Table D.4
Checklist based on the *ARRIVE Essential 10*. N/A stands for Not Applicable. Since this is a descriptive (exploratory) experiment designed to observe the correlation between ICP and EEG previous and during ICH episodes, concepts such as Blinding, Randomization, and Exclusion/Inclusion criteria are not applicable.

Item	(Sub)Section
Ethical statement	*2.1. Intracranial pressure experiment*
Study design	*Appendix A. Description of the experiment*
Sample size	*Appendix A. Description of the experiment*
Exclusion/Inclusion criteria	N/A
Randomization	N/A
Blinding	N/A
Outcome measures	*2.1. Intracranial pressure experiment*
Statistical methods	*2.2. EEG features calculation*
	2.3. Generalized additive model and classification performance
Experimental animals	*Appendix A.1. Animal preparation*
Experimental procedures	*Appendix A. Description of the experiment*
Results	*3. Results*

References

[1] C. Lazaridis, F.D. Goldenberg, Intracranial pressure in traumatic brain injury: from thresholds to heuristics, Crit. Care Med. 48 (8) (2020) 1210–1213.
[2] G.W. Hawryluk, G. Citerio, P. Hutchinson, A. Kolias, G. Meyfroidt, C. Robba, N. Stocchetti, R. Chesnut, Intracranial pressure: current perspectives on physiology and monitoring, Intensive Care Med. 48 (10) (2022) 1471–1481.
[3] R.M. Chesnut, N. Temkin, N. Carney, S. Dikmen, C. Rondina, W. Videtta, G. Petroni, S. Lujan, J. Pridgeon, J. Barber, et al., A trial of intracranial-pressure monitoring in traumatic brain injury, N. Engl. J. Med. 367 (26) (2012) 2471–2481.

[4] H. Hoffman, K. Abi-Aad, K.M. Bunch, T. Beutler, F.O. Otite, L.S. Chin, Outcomes associated with brain tissue oxygen monitoring in patients with severe traumatic brain injury undergoing intracranial pressure monitoring, J. Neurosurg. 135 (6) (2021) 1799–1806.
[5] S. Stein, R. Sonnenschein, Some relationships between intracranial pressure and EEG frequency in cats, Proc. Soc. Exp. Biol. Med. 82 (3) (1953) 509–511.
[6] S. Notermans, S. Boonstra, Electroencephalographic findings in experimentally induced intracranial hypertension, Electroencephalogr. Clin. Neurophysiol. 27 (4) (1969) 337–345.
[7] F.M. Forster, L.F. Nims, Electroencephalographic effects of acute increases of intracranial pressure, Arch. Neurol. Psychiatry 47 (3) (1942) 449–453.
[8] T.W. Langfitt, H.M. Tannanbaum, N.F. Kassell, H. Zaren, Acute intracranial hypertension, cerebral blood flow, and the EEG, Electroencephalogr. Clin. Neurophysiol. 20 (2) (1966) 139–148.
[9] J.-L. Vincent, Annual Update in Intensive Care and Emergency Medicine 2012, Springer Science & Business Media, 2012.
[10] N.M. Ciarrocchi, F. Pose, P. Saez, M. del Carman Garcia, F. Padilla, P. Plou, S. Hem, J.G. Karippacheril, A.F. Gutierrez, F.O. Redelico, Reversible focal intracranial hypertension swine model with continuous multimodal neuromonitoring, J. Neurosci. Methods 373 (2022) 109561.
[11] N.P. Du Sert, A. Ahluwalia, S. Alam, M.T. Avey, M. Baker, W.J. Browne, A. Clark, I.C. Cuthill, U. Dirnagl, M. Emerson, et al., Reporting animal research: explanation and elaboration for the arrive guidelines 2.0, PLoS Biol. 18 (7) (2020) e3000411.
[12] T. Hastie, R. Tibshirani, Generalized Additive Models, Wiley Online Library, 1990.
[13] P.H.C. Eilers, B.D. Marx, Flexible smoothing with *b*-splines and penalties, Stat. Sci. 11 (2) (1996) 89–102, http://www.jstor.org/stable/2246049.
[14] T. Hastie, Gam: generalized additive models, R package version 1.06.2, http://CRAN.R-project.org/package=gam, 2011.
[15] R Development Core Team, R: A Language and Environment for Statistical Computing, R Foundation for Statistical Computing, Vienna, Austria, ISBN 3-900051-07-0, 2012, http://www.R-project.org/.
[16] C. Robba, F. Graziano, P. Rebora, F. Elli, C. Giussani, M. Oddo, G. Meyfroidt, R. Helbok, F.S. Taccone, L. Prisco, et al., Intracranial pressure monitoring in patients with acute brain injury in the intensive care unit (synapse-icu): an international, prospective observational cohort study, Lancet Neurol. 20 (7) (2021) 548–558.
[17] D.A. Godoy, J. Carrizosa, S. Aguilera, W. Videtta, M. Jibaja, LABIC Members, Current practices for intracranial pressure and cerebral oxygenation monitoring in severe traumatic brain injury: a Latin American survey, Neurocrit. Care 38 (1) (2023) 171–177.
[18] N. Ciarrocchi, F. Pose, C.G. Videla, M. del Carmen García, F.D. Goldenberg, C. Lazaridis, N.P. Issa, F.O. Redelico, A. Mansour, Novel EEG metric correlates with intracranial pressure in an animal model, Neurocrit. Care (2023) 1–13.
[19] F. Pose, C. Videla, G. Campanini, N. Ciarrocchi, F.O. Redelico, Using entropies to monitoring intracranial pressure, evidence from an animal model, Biomed. Signal Process. Control 86 (2023) 105320.
[20] F. Pose, N. Ciarrocchi, C. Videla, F.O. Redelico, Permutation entropy analysis to intracranial hypertension from a porcine model, Entropy 25 (2) (2023) 267.
[21] A. Sanz-García, M. Pérez-Romero, J. Pastor, R.G. Sola, L. Vega-Zelaya, F. Monasterio, C. Torrecilla, G. Vega, P. Pulido, G.J. Ortega, Identifying causal relationships between EEG activity and intracranial pressure changes in neurocritical care patients, J. Neural Eng. 15 (6) (2018) 066029.
[22] A. Sanz-Garcia, M. Perez-Romero, J. Pastor, R.G. Sola, L. Vega-Zelaya, F. Monasterio, C. Torrecilla, G. Vega, P. Pulido-Rivas, G.J. Ortega, Is it possible to extract intracranial pressure information based on the EEG activity?, Rev. Neurol. 68 (9) (2019) 375–383.
[23] M. Connolly, P. Vespa, N. Pouratian, N.R. Gonzalez, X. Hu, Characterization of the relationship between intracranial pressure and electroencephalographic monitoring in burst-suppressed patients, Neurocrit. Care 22 (2015) 212–220.
[24] J. Claassen, L.J. Hirsch, K.T. Kreiter, E.Y. Du, E.S. Connolly, R.G. Emerson, S.A. Mayer, Quantitative continuous EEG for detecting delayed cerebral ischemia in patients with poor-grade subarachnoid hemorrhage, Clin. Neurophysiol. 115 (12) (2004) 2699–2710.
[25] D. Cardim, B. Schmidt, C. Robba, J. Donnelly, C. Puppo, M. Czosnyka, P. Smielewski, Transcranial Doppler monitoring of intracranial pressure Plateau waves, Neurocrit. Care 26 (2017) 330–338.
[26] C. Robba, S. Bacigaluppi, D. Cardim, J. Donnelly, A. Bertuccio, M. Czosnyka, Non-invasive assessment of intracranial pressure, Acta Neurol. Scand. 134 (1) (2016) 4–21.
[27] K.-H. Kim, H. Kim, K.-J. Song, S.-D. Shin, H.-C. Kim, H.-J. Lim, Y. Kim, H.-J. Kang, K.-J. Hong, Prediction of increased intracranial pressure in traumatic brain injury using quantitative electroencephalogram in a porcine experimental model, Diagnostics 13 (3) (2023) 386.
[28] B.M. Bolker, M.E. Brooks, C.J. Clark, S.W. Geange, J.R. Poulsen, M.H.H. Stevens, J.-S.S. White, Generalized linear mixed models: a practical guide for ecology and evolution, Trends Ecol. Evol. 24 (3) (2009) 127–135.
[29] C. Robba, S. Pozzebon, B. Moro, J.-L. Vincent, J. Creteur, F.S. Taccone, Multimodal non-invasive assessment of intracranial hypertension: an observational study, Crit. Care 24 (1) (2020) 1–10.
[30] K. Thibault, S. Margulies, Age-dependent material properties of the porcine cerebrum: effect on pediatric inertial head injury criteria, J. Biomech. 31 (1998) 1119–1126.
[31] K. Purins, A. Sedigh, C. Molnar, L. Jansson, O. Korsgren, T. Lorant, G. Tufveson, L. Wennberg, L. Wiklund, A. Lewén, P. Enblad, Standardized experimental brain death model for studies of intracranial dynamics, organ preservation, and organ transplantation in the pig, Crit. Care Med. 39 (2011) 512–517.
[32] A. Goldberg, The principles of humane experimental technique: is it relevant today?, ALTEX (2010) 149–151, https://doi.org/10.14573/altex.2010.2.149.
[33] N. Percie du Sert, V. Hurst, A. Ahluwalia, S. Alam, M.T. Avey, M. Baker, W.J. Browne, A. Clark, I.C. Cuthill, U. Dirnagl, et al., The ARRIVE guidelines 2.0: updated guidelines for reporting animal research, J. Cereb. Blood Flow Metab. 40 (9) (2020) 1769–1777.
[34] N.B. Robinson, K. Krieger, F.M. Khan, W. Huffman, M. Chang, A. Naik, R. Yongle, I. Hameed, K. Krieger, L.N. Girardi, et al., The current state of animal models in research: a review, Int. J. Surg. 72 (2019) 9–13.
[35] J. Karippacheril, T. Ho, Data acquisition from S/5 GE Datex anesthesia monitor using VSCapture: an open source.NET/Mono tool, J. Anaesthesiol. Clin. Pharmacol. 29 (3) (2013) 423, https://doi.org/10.4103/0970-9185.117096.